ISBN: 978-628-96613-1-6. ISSN: 2414-6390. Digital Object Identifier: https://dx.doi.org/10.18687/LACCEI2025.1.1.1498

# Thermal Monitoring of $LiFePO_4$ Lithium Battery System for the Use of an Electric Boat with Recharging Based on Photovoltaic Systems.

Julio Fredy Chura Acero[1]; Norman Jesús Beltrán Castañon[2]; Wilson Percy Clavetea Meneses[3]; Omar Chayña Velasquez[4]; Armando Tito Cruz Cabrera[5]; Katia Pérez Argollo[6]; Mateo Alejandro Salinas Mena[7]
[1,2,3,4,5,6,7]Universidad Nacional del Altiplano Puno, Perú, jchura@unap.edu.pe, nbeltran@unap.edu.pe, wclavetea@unap.edu.pe, ochayna@unap.edu.pe, armandocruz@unap.edu.pe, kperez@unap.edu.pe, msalinasm@unap.edu.pe

***Abstract*– For the safe operation and control of battery deterioration, thermal monitoring is extremely important. The performance of a battery energy system and its accuracy in State of Charge (SoC) (%) estimation for electric boats and electric vehicles are significantly influenced by ambient temperature. In this study, the battery will operate at extreme temperatures within Titicaca Lake, located at an altitude of 3850 meters above sea level. Therefore, the objective is to study a battery model that considers ambient and extreme temperatures. The cell must operate at critical values with a current of 150 A, a voltage of 3.65 V, and observe thermal aging that affects the capacity due to multiple charges and discharges. The method applied to lithium iron phosphate batteries LiFePO4 involved wear testing, considering three stress factors (time, temperature, and state of charge (SoC) (%)). Capacity measurements and resistance calculations tracked short-term degradation behaviors. The Shepherd model was established to identify battery aging using a simple but accurate two-step nonlinear regression approach; also, the thermal analysis of the battery cell was conducted to identify the most critical zone of the cell in terms of heat generation. This analysis allowed us to maximize heat dissipation with only a forced air fan mounted on the vital region. For further evaluation of the proposed strategies, a computational fluid dynamics (CFD) model was built in COMSOL Multiphysics® and validated with a thermographic camera to identify the temperature in the cells. The final arrangement of the LiFePO4 battery is the 16s1p prismatic cell type (16 cells in series and one parallel), with the cell experiencing a temperature variation of approximately 1° C higher than that of the outer parts.***

***Keywords*-- $LiFePO_4$ battery; electric boat; recharging; state of charge; battery thermal management; photovoltaic.***

## I. Introduction

Cathodes of $LiFePO_4$ lithium batteries represent the optimal choice for photovoltaic systems, as well as other renewable energy applications, aiming to achieve energy self-consumption [1]. Certain categories of lithium batteries exhibit specific attributes related to weight, dimensions, safety, and robustness, allowing them to adapt to scenarios where lead-acid batteries are not viable [2].

Lithium iron phosphate $LiFePO_4$ batteries represent a category of rechargeable lithium-ion batteries designed for high-power applications [3]. These batteries feature high discharge currents, lack explosiveness, exhibit a significant cycle life, and initially have lower energy density compared to lithium cobalt oxide, but surpass it significantly by the third year due to their greater stability [4].

### *A. Lithium Iron Phosphate LiFePO4*

In 1996, the University of Texas discovered that phosphate could be used as a cathode material for lithium batteries [5]. This cathode material remains stable even under overload conditions and can tolerate high temperatures without decomposing. The cathode material in lithium iron phosphate batteries is more reliable and safer than other cathode materials such as LiCoO2 or LiMn2O4 batteries [6]. Phosphates have a cell operating temperature range of -30°C to +60°C and a cell packaging temperature range of -50°C to +60°C, which reduces the risk of overheating and fire hazard [7]. This type of battery is made from nanoscale phosphate materials and exhibits low resistance, long lifespan, high capacity to handle heavy loads, improved safety and thermal consistency, no toxic effects, and lower cost. It has a reduced impact on cycle life concerning overcharge and undercharge, although specific energy slightly decreases compared to LiMn2O4. It exhibits some negative performance and lifespan properties due to temperature [8]. Lithium-phosphate batteries are capable of providing a specific energy and nominal voltage of approximately 160 mAh/g and 3.40 V, respectively [9]. These characteristics make it straightforward to enhance battery performance. Within lithium ion batteries, according to its chemical composition, LFP (LiFePO4) is the cathode source, see Figure 1, illustrates the types of cells for design and chemistry [10].

### *B. Reaction of Lithium Iron Phosphate LiFePO4 Battery Chemical*

A new type of high-performance battery is the lithium iron phosphate $LiFePO_4$ battery. An electrochemical process underlies its chemical reaction mechanism [11]. It has been extensively utilized in energy storage systems and electric boat because of its benefits, which include high energy density, extended cycle life, and environmental friendliness [12].

The two primary components of the chemical process in a lithium iron phosphate $LiFePO_4$ battery are the charging reaction and the discharging reaction [13].

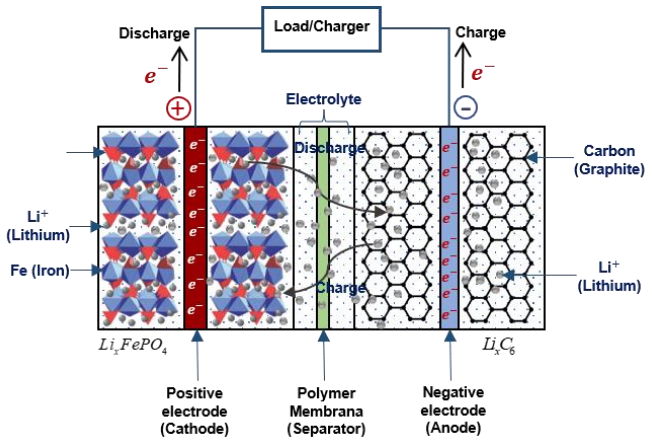


Fig. 1 Charging-discharging process of a LiFePO4 type battery

In the process of charging, the positive electrode (lithium iron phosphate) undergoes a reaction where it relinquishes oxygen molecules, converting them into iron trioxide (Fe203), and simultaneously discharges electrons, see Eq. 1. Conversely, the negative electrode (graphite) assimilates electrons and transforms lithium ions into metallic lithium [14], [15]. The process is shown in Figure 1.

Positive reaction:

$$LiFePO_4 \rightleftharpoons Li_{1-x}FePO_4 + xLi^+ + xe^- \quad (1)$$

Negative reaction:

$$xLi^+ + xe^- + 6C \rightleftharpoons Li_xC_6 \quad (2)$$

Total reaction:

$$LiFePO_4 + 6C \rightleftharpoons Li_{1-x}FePO_4 + Li_xC_6 \quad (3)$$

LiFePO4 is the chemical formula of lithium iron phosphate; in the Eq. 1. $Li_{1-x}FePO_4$ is a vacancy-containing chemical compound; $xLi^+$ represents lithium ions that have lost $x$ electrons; $xe^-$ represents the $x$ electrons released; and $6C$ is the chemical formula of graphite.

When the battery is charged, lithium ions move from the positive electrode to the negative electrode, where they react chemically with graphite and cling to the graphite's surface, forming lithium compounds. At the same time, electrons in the battery travel from the positive to negative electrodes, producing current in the external circuit. As a result, lithium iron phosphate batteries have high energy density, a long cycle life, and are environmentally friendly, making them promising for use in the field of renewable energy.

## II. The Operational Environment of an Electric Boat

### *2.1 Power System Structure*

An autonomous electric boat is being constructed with photovoltaic systems and a special nautical lithium battery that enhances the protection and performance of this electric vessel. It measures 7.5 meters in length from bow to stern, 2.20 meters in width, and is powered by a NAVY 6.0 electric motor with 9.9 HP, 39-60 V dc. It uses a $LiFePO_4$ lithium-ion battery model E-163 with 8345 Wh and 163 Ah capacity, charged by a CH4200 lithium battery charger of 30A, 220V AC 1440 W. The boat also features a solar charge controller for the E-series 48 V battery, 1600 W, and a photovoltaic system with 6 Monocrystalline RenePV 24 V dc, 270 W, Voltage at Pmax of 31.35V and Current at Pmax of 8.61A.

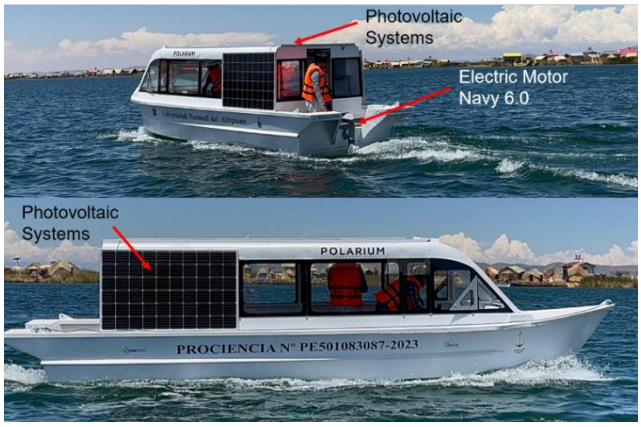


Fig. 2 Here we can see the electric boat in operation with the LiFePO4 lithium-ion battery model E-163, NAVY 6.0 electric motor, Photovoltaic system, Charged 30A serie CH4200

The choice of the electrical system depends on various factors such as the aquatic environment, navigation conditions, and economic costs. This document considers the basic structure of the hull, vessel, or outer lining that wraps around and waterproofs its framework, forming the hull and the cabin area where the photovoltaic system is mounted. When the electric boat docks, it is powered from the 220 V electrical grid with a transformer capacity of 10 kVA. Single-phase industrial simple charging point, type 1 up to 125 A, SAE J1772/IEC 62196-2, considered within the Battery Electric Vehicle (BEV) technology, which is a fully electric vehicle powered exclusively by a lithium battery.

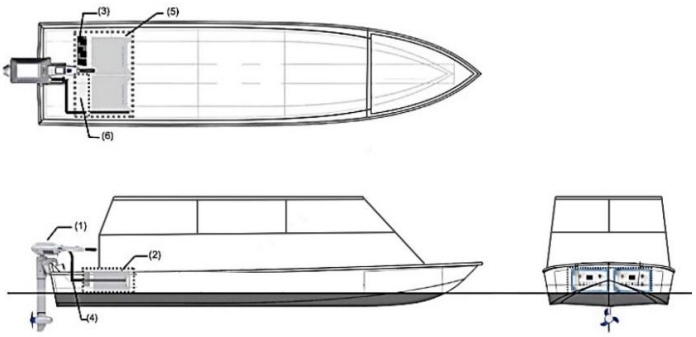


Fig. 3 This is a figure. Schemes follow the same formatting. If there are multiple panels, they should be listed as: (1) NAVY 6.0 electric motor, (2) LiFePO4 lithium-ion battery model E-163, (3) Charged 30 A serie CH4200, 4) Power and data cable (5) Drawer for the system (battery, charger and wiring), (6) secondary drawer for charging cable.

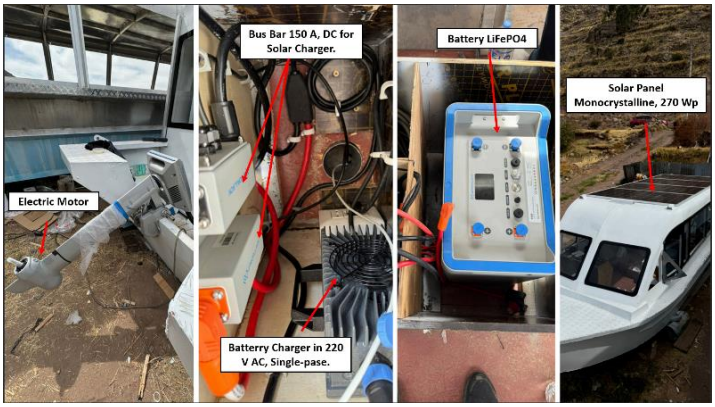


Fig. 4 Parts that make up the propulsion system.

The primary propulsion engine that powers the propeller must adhere to all applicable regulations or standards set out by the maritime inspection organization. These include those pertaining to the marine motor, motor protection class, insulation level, and other technical indications. Furthermore, the motor needs to function properly in environments with mildew, oil, salt, and damp air. To prevent motor blockages due to propeller windings, the motor needs to have a one-minute overload capacity. The motor's speed range need to be sufficient for the propeller's needs. The DC motor has low cost, good durability, and simplicity.

When operating at full speed, the motor's rated power should match the propulsion's rated power. In the Figure 5 displays the motor's primary technical specifications.

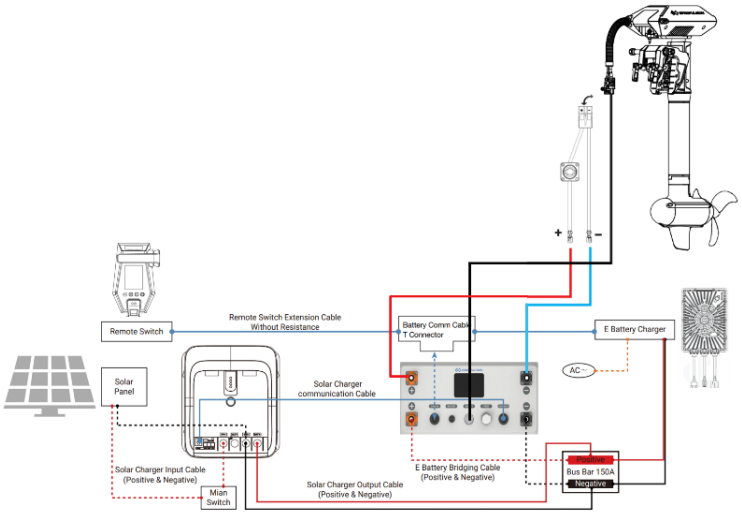


Fig. 5 Components of the propulsion system for the electric boat of the project; solar panel, solar charger, remote switch, battery LiFePO4, motor, battery charger

*2.2 Battery Experiment*

The capacity of prismatic $LiFePO_4$ cells typically ranges from 100 to 300 Ah. This capacity range makes them suitable for applications requiring moderate to high energy storage capacity, such as electric vehicles (EVs), energy storage systems (ESS) for residential or commercial use, and industrial applications.

A commercial $LiFePO_4$ battery with a capacity of 163 Ah, 3.2 V is used in this investigation, is an aluminum-cased lithium iron phosphate prismatic battery that is ideal for power applications such as electric vehicles and boats.

## III. Result and Analysis

*3.1 Result of Temperature behavior for $LiFePO_4$ prismatic cells*

Heat transfer in fluids in vector form can be described using the concept of heat flux, which is a vector quantity indicating the amount of heat crossing a surface per unit time and area. In vector terms, heat transfer in fluids is expressed as:

$$\vec{q} = -k \cdot \nabla T \quad (4)$$

where; $\vec{q}$ is the heat flux vector, indicating direction and magnitude, $k$ is the thermal conductivity of the fluid, $\nabla T$ is the temperature gradient, a vector indicating the direction and rate of temperature change in space.

In the Eq. 4, The negative sign indicates that heat flux always moves from regions of higher temperature to regions of lower temperature, in accordance with the second law of thermodynamics. $k \cdot \nabla T$ represents the amount of heat flowing through a surface per unit area and time, where $\nabla T$ defines the direction and magnitude of the temperature gradient.

In the equation 5, this vectorial model is fundamental for formulating and solving heat transfer problems in fluids, especially in applications where the direction and spatial distribution of heat within a fluid system are considered; $\rho$ density, $C_p$ specific heat, $\vec{u}$ Velocity Vector, $\vec{q}$ Heat flux by conduction, $Q$ Heat source, $Q_{ted}$ Thermoelastic effects. (M. Soltani *et al.* 2019). (J. Jaguemont *et al.* 2016).

$$\rho C_p \frac{\partial T}{\partial t} + \rho C_p \vec{u} \cdot \nabla T + \nabla \cdot \vec{q} = Q + Q_{ted} \quad (5)$$

COMSOL Multiphysics® created the 3D-thermal model to determine the cell's thermal behavior. An energy balance equation is used to specify the transient thermal distribution within the cell. This equation formulates the quantity of thermal energy that the cell generates for its surroundings as follows. (M. Soltani *et al.* 2019).

$$mC_p \frac{\partial T}{\partial t} + q_{conv} = k\left[\frac{\partial^2 T}{\partial x^2} + \frac{\partial^2 T}{\partial x^2} + \frac{\partial^2 T}{\partial x^2}\right] + q_g \quad (6)$$

where mass, heat capacity, temperature, thermal conductivity, and heat generation are denoted by the letters $m$, $C_p$, $T$, $k$, and $q_g$, respectively. In this paper, the polarization process and the cell's ohmic resistance are used to compute the heat generation of the cell. Additionally, Eq. (7) makes use of the tab domain.

$$q_g = R_{bt} \cdot I^2 + R_1 \cdot I_1^2 + R_2 \cdot I_2^2 \quad (7)$$

wherein, $I$ and $R_{bt}$ represent the current and ohmic resistance of the cell. (J. Jaguemont *et al.* 2016)

$$q_{conv} = hS(T_{amb} - T) \quad (8)$$

where $h$ and $S$ stand for the cell's cross section area and coefficient of heat transfer, respectively. $T_{amb}$ and $T$ also show the battery and the surrounding temperature. A thermal camera clearly shows that the temperature distribution within the cell region is not uniform in Fig. 6.

According to the model described in Eq. 4 and 5, you can see the simulation for the prismatic lithium cells; within the cell, there is a negligible variation in temperature. As would be predicted given that this is the location that is farthest from the cooling surfaces, the highest temperature is reached within the jelly roll, about in the center of the cell. During discharge and charging, the temperature rises; that is, it does not attain a constant state. See the figures 6 to 8.

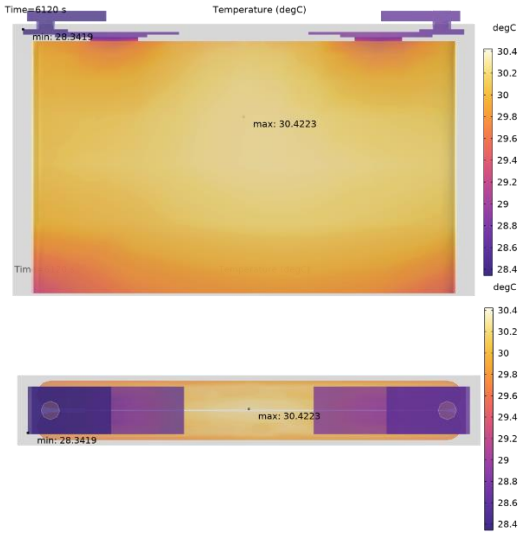


Fig. 6 This is a figure of Temperature Field of prismatic lithium cell, simulated in COMSOL.

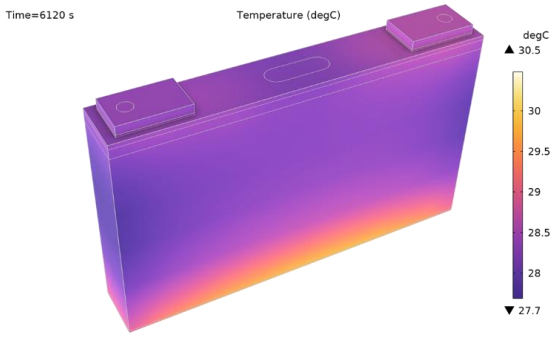


Fig. 7 Surface temperature, simulated in COMSOL

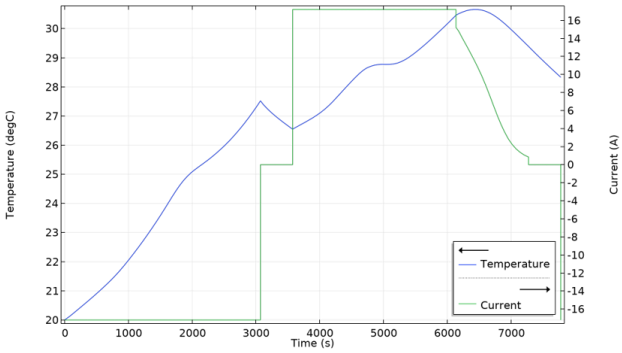


Fig. 8 The temperature increases during discharge and charge.

The significance of the metal foils in cooling the cell is seen by the temperature along the roll layer's cross sections at that location. The temperature displays a local maximum on the negative current collector foil and a local minimum on the positive foil. The cell's outside cooling is the cause of the minimum. Since it is the layer farthest from the cooling tab, the maximum is. At the location of the negative foil, an

identical but opposite effect is observed. The nearest foil that is closest to a tab tends to chill the jelly roll layer's components.

Finally the variance in external temperature is a result of the disparity in thermal conductivity between the metal components and the electrical insulators. The bottom of the cell, where the jelly roll and battery container are in close contact, has the highest temperature. See the Figure 7.

*3.2 Result of external temperature behavior for the prismatic $LiFePO_4$ (16 cells in series and one parallel cells)*

The thermographic camera monitors the first charging process of the photovoltaic system and the discharge of the battery to the electric motor, providing information about the temperature distribution and potential short circuits. The automatic detection of hot spots recognizes and automatically reports deviations from the target temperature.

Hot spots in batteries during operation can provide an indication of the areas where the battery will fail. This adverse thermal behavior can quickly spread throughout the battery in a domino effect known as thermal runaway, which can lead to catastrophic failures. Excessive voltage, charge, ambient temperature, or a combination of these factors can trigger thermal runaway. Sealed cells can sometimes explode violently if the safety vents become clogged or fail to function. Lithium-ion batteries are particularly prone to thermal runaway.

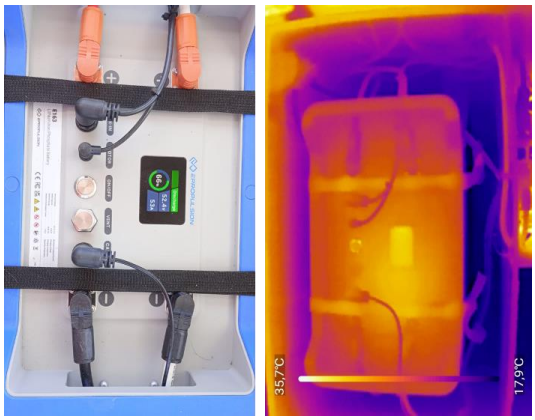


Fig. 9 External temperature behavior for the prismatic LiFePO4 (16 cells in series and one parallel cells).

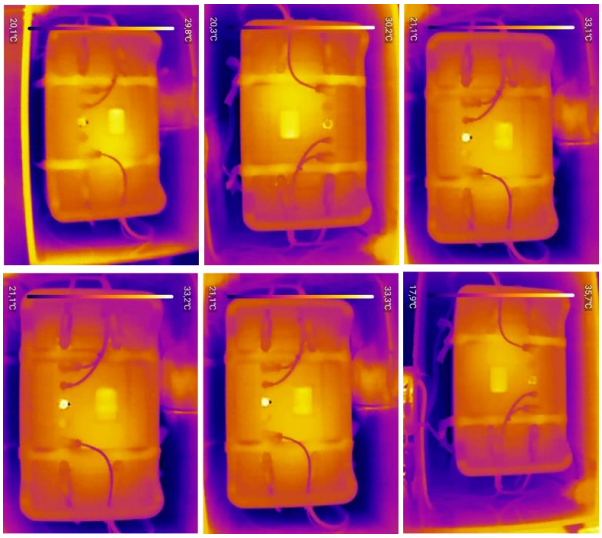

Fig. 10 The temperature increases during discharge and charge 29.8 ˚C to 35.7˚ C.

The cell's temperature under natural air cooling is taken into account for the beginning temperatures of 20.1 ˚C to 35.7 ˚C at a 53 Amp. discharging rate. However, during charging with the photovoltaic system, the temperature varies between 20 ˚C at a charging current of 13 A. See the Figures 9 and 10.

## IV. Conclusions

With the proposal to reduce polluting emissions from electric boats within the bay of Lake Titicaca, thereby improving air quality, flora, and fauna, this study presented a hybrid energy system powered by a photovoltaic DC system and conventional AC grid according to the characteristics reflected in current electromobility standards such as SAE J1772, IEC 61851, and GB/T 20234-2. A method for designing parameters of the hybrid energy system based on loads like the 6 kW, 9.9 HP propulsion motor and auxiliary equipment was suggested. The results of the experiments demonstrate that the proposed technique for designing system parameters and control strategy for the hybrid energy system are satisfactory; the energy capacity meets the navigation requirements on Lake Titicaca. The benefits of energy conservation and emission reduction are clearly evident.

Thermal modeling is an effective way to understand the thermal behavior of LiFePO4 lithium-ion batteries during charging and discharging. With charging and discharging, the internal heat generation of the battery increases, thereby raising its temperature with an uneven distribution and partial degradation of the battery.

Non-destructive evaluation of batteries using thermographic cameras allows for determining the temperature distribution in the lithium-ion battery. The key to solving the safety issue lies in thermal control, including heat generation and internal and external heat transfer. Therefore, a

model was created independently for each cell, capturing the geometric thermal effects on the thermal abuse behavior of the battery based on the charging of the photovoltaic system and discharge to the electric motor.

The analysis of discharge voltage characteristics in the prismatic cell type shows that comparing the rate of voltage changes in the final discharge phase will allow us to detect SoC imbalances. Parameters were obtained that will enable us to develop a damage protection system for the entire cell arrangement for $LiFePO_4$ batteries in 16S1P configuration.

## ACKNOWLEDGMENT

The authors would like to thank CONCYTEC-PROCIENCIA under contract number PE501083087-2023 and the Vice Rectorate of Research of the National University of the Altiplano Puno for their support and the provided motivation.

## REFERENCES

[1] Madej, W.; Wojciechowski, A. *Analysis of the charging and discharging process of LiFePO4 battery pack*. Energies 2021, 14. https://doi.org/10.3390/en14134055.

*[2]* Sui, X.; ´Swierczy ´nski, M.; Teodorescu, R.; Stroe, D.I. *The degradation behavior of lifepo4/c batteries during long-term calendar aging.* Energies 2021, 14. https://doi.org/10.3390/en14061732.

[3] Jiang, S. Estimating the State of Health of Lithium-Ion Batteries with a High Discharge Rate through Impedance 2021.

[4] Neupane, S.; Alipanah, M.; Barnes, D.; Li, X. *Heat generation characteristics of LiFePO4 pouch cells with passive thermal management.* Energies 2018, 11. https://doi.org/10.3390/en11051243.

[5] Chin, C.S.; Gao, Z.; Chiew, J.H.K.; Zhang, C. *Nonlinear temperature-dependent state model of cylindrical LiFePO4 battery for open-circuit voltage, terminal voltage and state-of-charge estimation with extended kalman filter*. Energies 2018, 11. https://doi.org/10.3390/en11092467.

[6] Zhang, Z.; Lu, L.; Li, Y.; Wang, H.; Ouyang, M. *Accurate Remaining Available Energy Estimation of LiFePO4 Battery in Dynamic Frequency Regulation for EVs with Thermal-Electric-Hysteresis Model.* Energies 2023, 16. https://doi.org/10.3390/en16135239.

[7] Lu, Z.; Wang, Q.; Xu, F.; Fan, M.; Peng, C.; Yan, S. *Double-Layer SOC and SOH Equalization Scheme for LiFePO4 Battery Energy Storage System Using MAS Blackboard System.* Energies 2023, 16. https://doi.org/10.3390/en16145460.

[8] Vinci, G.; Arangia, V.C.; Ruggieri, R.; Savastano, M. *Reuse of Lithium Iron Phosphate ( LiFePO 4 ) Batteries from a Life Cycle Assessment Perspective : The Second-Life Case Study 2024.* pp. 1–19.

*[9]* Anr, L.; Pizarro-carmona, V.; Cort, M.; Palma-behnke, R.; Calder, W.; Orchard, M.E.; Est, P.A. *An Optimized Impedance Model for 307*

[10]*the Estimation of the State-of-Charge of a Li-Ion Cell* : The Case of a 2019. 4. https://doi.org/10.3390/en12040681.

[11]Gatta, F.M.; Geri, A.; Lamedica, R.; Lauria, S.; Maccioni, M.; Palone, F.; Rebolini, M.; Ruvio, A. *Application of a LiFePO 4 Battery Energy Storage System to Primary Frequency Control : Simulations and Experimental Results 2016*. https://doi.org/10.3390/ 310 en9110887. 311

[12]Hua, Y.; Xu, M.; Li, M.; Ma, C.; Zhao, C. *Estimation of State of Charge for Two Types of Lithium-Ion Batteries by Nonlinear Predictive Filter for Electric Vehicles* 2015. pp. 3556–3577. https://doi.org/10.3390/en8053556. 313

*[13]* Liu, X.; Gao, Y.; Marma, K.; Miao, Y.; Liu, L. *Advances in the Study of Techniques to Determine the Lithium-Ion Battery ' s State of Charge 2024.*

[14]Hannan, M.A.; Hoque, M.M.; Hussain, A.; Yusof, Y.; Ker, P.J. *State-of-the-Art and Energy Management System of Lithium-Ion Batteries in Electric Vehicle Applications: Issues and Recommendations*. IEEE Access 2018, 6, 19362–19378. https://doi.org/10.1109/ACCESS.2018.2817655. 318

[15]Aksoz, A.; Asal, B.; Biçer, E.; Oyucu, S.; Gençtürk, M.; Golestan, S. *Advancing Electric Vehicle Infrastructure* : A Review and 2024.

[16]Stanko, P.; Tkac, M.; Kajanova, M.; Roch, M. *Impacts of Electric Vehicle Charging Station with Photovoltaic System and Battery Energy Storage System on Power Quality in Microgrid* 2024.

[17]Zhou, Z.; Duan, B.; Kang, Y.; Zhang, Q.; Shang, Y.; Zhang, C. *Online State of Health Estimation for Series-Connected LiFePO4 Battery Pack Based on Differential Voltage and Inconsistency Analysis*. IEEE Transactions on Transportation Electrification 2024, 10, 989–998. https://doi.org/10.1109/TTE.2023.3274819. 324

[18]Qays, M.O.; Buswig, Y.; Hossain, M.L.; Rahman, M.M.; Abu-Siada, A. *Active cell balancing control strategy for parallelly connected LiFePO4batteries*. CSEE Journal of Power and Energy Systems 2021, 7, 86–92. https://doi.org/10.17775/CSEEJPES.2020.00740.

[19]Gao, D.; Zhang, W.; Shen, A.; Wang, Y. *Parameter Design and Energy Control of the Power Train in a Hybrid Electric Boat* 2017. pp. 1–12. https://doi.org/10.3390/en10071028.

[20]Acero, J.F.C.; Castañon, N.J.B.; Yucra, R.C.; Viveros, H.P.; Coaquira, A.M.L. *Harmonics of the Microinverters for the Operation of the Grid-Connected Photovoltaic Energy System Considering the Uncertainty of Irradiance*. In Proceedings of the Proceedings of the 7th Brazilian Technology Symposium (BTSym'21). https://doi.org/10.1007/978-3-031-08545-1_68

[21]Li, Y.; Zhou, Z.; Su, L.; Bai, M.; Gao, L.; Li, Y.; Liu, X.; Li, Y.; Song, Y. *Numerical Simulations for Indirect and Direct Cooling of LiFePO4 Battery Pack*. Energies 2022, 15. https://doi.org/10.3390/en15134581. 335

[22]Z. Liao, S. Zhang, K. Li, G. Zhang, and T. G. Habetler, "*A survey of methods for monitoring and detecting thermal runaway of lithium-ion batteries,"* J. Power Sources, vol. 436, Oct. 2019, Art. no. 226879.

[23]I. Alsaidan, W. Gao, and A. Khodaei, *"Optimal design of battery energy storage in stand-alone brownfieldmicrogrids"* inProc.NorthAmer.Power Symp., Morgantown, WV, USA, Sep. 2017, pp. 1–6.

[24]Z. Miao, L. Xu, V. R. Disfani, and L. Fan, "*An SOC-based battery managementsystemformicrogrids*" IEEETrans. SmartGrid,vol.5,no.2, pp. 966–973, Mar. 2014.

[25]M.T.Lawderet al., "*Battery energy storage system (BESS) and battery management system (BMS) for grid-scale applications,"* Proc. IEEE, vol. 102, no. 6, pp. 1014–1030, Jun. 2014.

[26]M. Bragard, N. Soltau, S. Thomas, and R. W. De Doncker, "*The balance of renewable sources and user demands in grids: Power electronics for modular battery energy storage systems,"* IEEE Trans. Power Electron., vol. 25, no. 12, pp. 3049–3056, Dec. 2010.

[27]D. Anseán, M. González, V. M. García, J. C. Viera, J. C. Antón, and C. Blanco, *"Evaluation of LiFePO4 batteries for electric vehicle appli cations,"* IEEE Trans. Ind. Appl., vol. 51, no. 2, pp. 1855–1863, Mar. Apr. 2015.

[28]M.Einhorn,F.V.Conte,C.Kral,andJ.Fleig,*"Comparison,selection, and parameterization of electrical battery models for automotive applications,"* IEEE Trans. Power Electron., vol. 28, no. 3, pp. 1429–1437, Mar. 2013.

[29]S. Buller, M. Thele, E. Karden, and R. W. D. Doncker, "Impedance-based non-linear dynamic battery modeling for automotive applications," J. Power Sources, vol. 113, no. 2, pp. 422–430, Jan. 2003.

[30]A. E. Mejdoubi, H. Gualous, H. Chaoui, and G. Alcicek, "Experimental investigation of calendar aging of lithium-ion batteries for vehicular appli cations," in Proc. EMC Conference, Turkiye, Ankara, Sep. 2017, pp. 1–5.

[31]M.Sayegh,C.Forgez,T.H.Tran,andG.Cherouvrier,"LiFePO4/graphite battery modelling for an aeronautical application," in Proc. IEEE 24th Int. Symp. Ind. Electron., Jun. 2015, pp. 1278–1283.

[32]J. P. Fellner, G. J. Loeber, S. P. Vukson, and C. A. Riepenhoff, "Lithium ion testing for spacecraft applications," J. Power Sources, vol. 119–121, pp. 911–913, 2003.

[33]GianfrancoPistoia,InBatteryOperatedDevicesandSystems.Amsterdam, The Netherlands: Elsevier, 2009.

[34]H. Rahimi-Eichi, U. Ojha, F. Baronti, and M. Y. Chow, “Battery manage ment system: An overview of its application in the smart grid and electric vehicles,” IEEE Ind. Electron. Mag., vol. 7, no. 2, pp. 4–16, Jun. 2013.
[35]J. Cao, N. Schofield, and A. Emadi, “Battery balancing methods: A comprehensive review,” in Proc. IEEE Veh. Power Propulsion Conf.,Sep. 2008, pp. 1–6.
[36]D. Linden and T. Reddy, Handbook of Batteries, 3rd ed. New York, NY, USA: McGraw-Hill Professional, 2001.
[37]B. Weißhar and W. G. Bessler, “Model-based degradation assessment of lithium-ion batteries in a smart microgrid,” in Proc. Int. Conf. Smart Grid Clean Energy Technol., Oct. 2015, pp. 134–138.
[38]J. C. Koo, S. K. Lee, and S. W. Ra, “Lithium-ion battery design for the hybrid satellite in the geostationary orbit,” in Proc. Int. Telecommun. Energy Conf., Dec. 2009, pp. 1–6.
[39]D.A.González,“HighpowerLi-IONbatteryperformance:Amechanistic analysis of aging,” Ph.D. thesis, Dept. Elect., Electron., Comput. Syst. Eng., University of Oviedo, Oviedo, Spain. 2015. [Online]. Available: http://hdl.handle.net/10651/34551. Accessed on: Jan. 16, 2018.
[40]C.D.RahnandC.-Y.Wang,Battery Systems Engineering, 1st ed. Oxford, U.K.: Wiley, 2013.
[41]Markets and markets, “Lithium Ion Battery Market- Global Forecast to 2025,” Jan. 2019. [Online]. Available: https://www.marketsandmarkets. com/Market-Reports/lithium-ion-battery-market-49714593.html. Accessed on: Oct. 30, 2019.
[42]M. A. Roscher and D. U. Sauer, “Dynamic electric behavior and open circuit-voltage modeling of LiFePO4-based lithium ion secondary batter ies,” J. Power Sources, vol. 196, pp. 331–336, Jan. 2011.
[43]F. Feng, R. Lu, G. Wei, and C. Zhu, “Identification and analysis of model parameters used for LiFePO4 cells series battery pack at various ambient temperature,” IET Elect. Syst. Transport., vol. 6, no. 2, pp. 50–55, May 2016.
[44]M.Takahashi, S. Tobishima, K. Takei, and Y. Sakurai, “Reaction behavior of LiFePO4 asacathodematerialforrechargeablelithiumbatteries,” Solid State Ionics, vol. 148, nos. 3–4, pp. 283–289, Jun. 2002.
[45]L. W. Juang, P. J. Kollmeyer, T. M. Jahns, and R. D. Lorenz, “Improved modeling of lithium-based batteries using temperature-dependent resis tance and overpotential,” in Proc. IEEE Transport. Electrific. Conf. Expo., Jun. 2014, pp. 1–8.
[46]M. Soltani, G. Berckmans, J. Jaguemont, J. Ronsmans, S. Kakihara, O. Hegazy, J. Van Mierlo, N. Omar, Three dimensional thermal model development and validation for lithium-ion capacitor module including air-cooling system, Appl. Therm. Eng. 153 (2019) 264–274, https://doi.org/10.1016/j.applthermaleng.2019.03.023.
[47]M. Soltani, J. Ronsmans, J. Jaguemont, J. Van Mierlo, P. Van Den Bossche, N. Omar, A Three-dimensional thermal model for a commercial lithium-ion capacitor battery pack with non-uniform temperature distribution, Proc. IEEE Int. Conf. Ind. Technol. 2019-Febru. 2019, pp. 1126–1131, , https://doi.org/10.1109/ICIT. 2019.8755081.
[48]J. Jaguemont, L. Boulon, Y. Dubé, Characterization and modeling of a hybridelectric-vehicle lithium-ion battery pack at low temperatures, IEEE Trans. Veh. Technol. 65 (2016) 1–14, https://doi.org/10.1109/TVT.2015.2391053.
[49]J. Francisco Lima Flores *et al.*, “Evaluation of the Efficiency and Control of a 250 W Solar Micro Inverter Connected to the Electrical Distribution Network Operating Above 3800 masl,” *Proc. LACCEI Int. Multi-conference Eng. Educ. Technol.*, pp. 1–6, 2024, doi: 10.18687/LACCEI2024.1.1.1816.